Structure and Chemical Inhibition of the RET Tyrosine Kinase Domain*

Phillip P. Knowles[‡], Judith Murray-Rust[‡], Svend Kjær[‡§1], Rizaldy P. Scott[§2], Sarah Hanrahan[‡], Massimo Santoro[¶], Carlos F. Ibáñez[§], and Neil Q. McDonald[‡||3]

From the [‡]Structural Biology Laboratory, London Research Institute, Cancer Research UK, London WC2A 3PX, United Kingdom, the [||]School of Crystallography, Birkbeck College, Malet Street, London WC1E 7HX, United Kingdom, the [§]Division of Molecular Neurobiology, Department of Neuroscience, Karolinska Institute, SE-171 77 Stockholm, Sweden, and the [¶]Istituto di Endocrinologia e Oncologia Sperimentale del Consiglio Nazionale delle Ricerche, Dipartimento di Biologia e Patologia Cellulare e Molecolare, Università di Napoli Federico II, 80131 Naples, Italy

The *RET* proto-oncogene encodes a receptor tyrosine kinase for the glial cell line-derived neurotrophic factor family of ligands. Loss-of-function mutations in *RET* are implicated in Hirschsprung disease, whereas activating mutations in *RET* are found in human cancers, including familial medullar thyroid carcinoma and multiple endocrine neoplasias 2A and 2B. We report here the biochemical characterization of the human RET tyrosine kinase domain and the structure determination of the non-phosphorylated and phosphorylated forms. Both structures adopt the same active kinase conformation competent to bind ATP and substrate and have a pre-organized activation loop conformation that is independent of phosphorylation status. In agreement with the structural data, enzyme kinetic data show that autophosphorylation produces only a modest increase in activity. Longer forms of RET containing the juxtamembrane domain and C-terminal tail exhibited similar kinetic behavior, implying that there is no *cis*-inhibitory mechanism within the RET intracellular domain. Our results suggest the existence of alternative inhibitory mechanisms, possibly in *trans*, for the autoregulation of RET kinase activity. We also present the structures of the RET tyrosine kinase domain bound to two inhibitors, the pyrazolopyrimidine PP1 and the clinically relevant 4-anilinoquinazoline ZD6474. These structures explain why certain multiple endocrine neoplasia 2-associated RET mutants found in patients are resistant to inhibition and form the basis for design of more effective inhibitors.

The *RET* (<u>re</u>arranged during <u>t</u>ransfection) gene was originally isolated as an oncogenic fusion protein in cell transformation assays (1). The *RET* proto-oncogene (2), on human chromosome 10q11.2, encodes a receptor tyrosine kinase (RTK)[4] (3–5) activated by members of the glial cell line-derived neurotrophic factor (GDNF) ligand family (GDNF, neurturin, artemin, and persephin) (6) in conjunction with a ligand-specific coreceptor (GFRα1–4) (7). RET signaling is essential for development, survival, and regeneration of many neuronal populations such as those in the enteric and sympathetic nervous systems (6) and the kidney (8, 9). The domain organization of RET is shown in Fig. 1*A*; orthologs exist from *Drosophila* to human and share a high degree of sequence similarity (90% in vertebrates) throughout the cytoplasmic domain and, to a lesser extent, within the extracellular region.

GDNF family ligands do not interact directly with RET; instead, signaling via RET depends on formation of a tripartite complex of RET, a GDNF family ligand, and its cognate glycosylphosphatidylinositol-linked GFRα (10, 11). In addition, ligand binding requires Ca^{2+} ions chelated to the RET extracellular domain (12, 13). According to the classical RTK paradigm, formation of the complex promotes RET dimerization, leading to *trans*-autophosphorylation within the RET intracellular domain (RET-ICD). There are two tyrosine residues (Tyr^{900} and Tyr^{905}) in the RET tyrosine kinase domain (RET-KD) activation loop (A-loop), both of which have been found to be autophosphorylation sites by mass spectrometry (14); Tyr^{905} has been shown to be required for RET downstream signaling (15). Phosphorylation at Tyr^{981}, Tyr^{1015}, Tyr^{1062}, and Tyr^{1096} has been shown to be of major importance for further signal propagation (16), and each forms a binding site for one or more downstream adaptor molecules (see Arighi *et al.* (11) for a recent review). *RET* has attracted considerable clinical interest

---

because of the range of mutations found in diverse conditions that include Hirschsprung disease and a variety of cancers involving the thyroid gland. *RET* is the gene most commonly mutated in patients with familial or sporadic Hirschsprung disease, which is characterized by deficiencies in the enteric nervous system and intestine malfunction (17, 18). *RET*-related cancers with thyroid involvement include sporadic and familial medullary thyroid carcinoma (MTC; OMIM #155240), multiple endocrine neoplasia 2 (MEN2; OMIM #171400) syndromes MEN2A and MEN2B, and papillary thyroid carcinoma (PTC).

To date, >100 mutations in the *RET* gene have been described, and with the exception of a few dual-phenotype mutations (19), they can be generally partitioned into loss- or gain-of-function groups. *RET* mutations in Hirschsprung disease are characterized by loss of function and can be broadly classified into three groups: extracellular residues that are essential for protein folding, the alteration of which leads to immature non-folded RET being retained in the endoplasmic reticulum (20); residues in RET-KD that adversely affect protein stability or activity (21, 22); and docking residues required for downstream signaling (23). *RET*-related cancers generally involve gain-of-function mutations in RET that can be divided into two groups: those affecting cysteine residues in the cysteine-rich domain and those altering residues in RET-KD. In the first group, the most frequently mutated residue found in MEN2A patients is Cys[634], where removal of one-half of an intramolecular disulfide bond allows formation of an intermolecular disulfide bond with a second mutant molecule, thus leading to constitutive receptor dimerization and aberrant signaling. Activating mutations within RET-KD are more varied in mechanism and not known to directly lead to constitutive dimer formation. A range of mutations such as L790F, Y791F, S891A, and R844L produce transforming RET, but with the relatively mild MTC and MEN2A phenotypes. In contrast, the M918T mutation has a very high transforming ability and is found in 95% of MEN2B patients (24). The MEN2B phenotype involves not only the thyroid and adrenal glands, but also a selection of mucosal, ocular, and skeletal abnormalities. M918T RET does not need Tyr[905] for activation, in marked contrast to the MEN2A dimerizing mutations, where Tyr[905] is required for oncogenesis (14, 24–27). This suggests that different underlying mechanisms subvert normal control of RET activation in MEN2A and MEN2B (28). In addition, M918T RET targets unique substrates such as STAT3 that may contribute to cell transformation (29, 30). As well as transforming mutations within intact *RET*, chromosome translocations can produce oncogenic fusions including the *RET* kinase domain (*RET*/*PTC* oncogenes) that give rise to PTC. RET/PTC fusion proteins are cytosolic and contain RET-KD from exon 12 (starting at Glu[713]) through to the C terminus (31). In many cases, the N-terminal domain of RET/PTC is a dimerization domain from the fusion partner. Notably, mutation of the residue in RET/PTC corresponding to Tyr[905] in wild-type RET leads to reduced transforming ability (32).

Because RET point mutations in familial MTC, MEN2A, and MEN2B and the RET/PTC fusions all result in inappropriate kinase activation, RET-KD presents a unique therapeutic target for treatment of the associated cancers (33, 34). Evidence for its suitability as a target comes from suppression of oncogenic RET in a thyroid carcinoma model system by small molecule inhibition (35) as well as from the beneficial effect of a dominant-negative RET mutant in MTC cells blocking tumor growth (36). Small molecule inhibitors of protein kinases have already been proven clinically useful for a variety of human diseases (37, 38). Potent inhibitors of wild-type RET and oncogenic forms have been described, including the pyrazolopyrimidines PP1 and PP2 and the 4-anilinoquinazoline ZD6474 (Zactima[TM]) (34). PP1 was first recognized as a Src family inhibitor, but also inhibits a number of RTKs (39), including RET (40). ZD6474 targets RET, vascular epidermal growth factor receptor (VEGFR), and epidermal growth factor receptor (EGFR) tyrosine kinases and is being tested in advanced trials against lung cancer as well as against locally advanced or metastatic hereditary MTC (41). The most oncogenic MEN2-associated RET-KD mutants are highly susceptible to PP1 and ZD6474 inhibition, with the exception of MEN2-associated V804L and V804M, which are resistant (42). A similar mutation of the analogous kinase "gatekeeper" residue of the *BCR-ABL* oncogene develops in imatinib-treated leukemia patients, thus requiring strategies to overcome inhibitor resistance (43).

In this study, we have expressed, purified, and biochemically characterized RET-KD and determined its structure in non-phosphorylated and phosphorylated forms. Both show the same interlobe orientation characteristic of active tyrosine kinases and have essentially identical A-loop conformations. We demonstrate that no major *cis*-inhibition mechanism operates within RET-ICD. We also describe the structural basis for inhibition of RET by PP1 and ZD6474 and how drug-resistant RET mutations ablate interaction with these inhibitors.

EXPERIMENTAL PROCEDURES

Recombinant Baculovirus Preparation and Protein Production—The cDNAs encoding RET-KD (residues 705–1013), RET-KD with its juxtamembrane domain (RET-JM-KD; residues 666–1013), and the entire RET-ICD (residues 666–1114) were PCR-amplified and subcloned into the HindIII and XhoI restriction sites of a modified pBacPak-His3 vector (Clontech). The modified vector contains a glutathione *S*-transferase (GST) coding region upstream of a 3C protease cleavage site. The RET-KD mutation Y905F was introduced by QuikChange mutagenesis (Stratagene) according to standard procedures. Generation of recombinant baculovirus was carried out according to the manufacturer's protocols (Clontech). The viruses were used to infect Sf9 cells with a multiplicity of infection of 5; cells were grown in shaker flasks in Grace's medium supplemented with 10% fetal bovine serum, 0.1% PLEURONIC F-68, and 10 μg/ml gentamycin. The cells were harvested 72 h post-infection and lysed by sonication. RET-KD was purified by incubation with glutathione-Sepharose 4B beads (Amersham Biosciences), followed by removal of the GST affinity tag using GST-linked 3C protease (PreScission protease, Amersham Biosciences). To produce phosphorylated RET-KD (RET-KD-P), 2.5 mM ATP and 5 mM MgCl$_2$ were added to the suspension at the same time as the PreScission protease. To generate nonphosphorylated RET-KD (RET-KD-0P), soluble RET-KD was treated with 1 unit of biotinylated alkaline phosphatase

(Sigma). Proteins were concentrated in Buffer A (20 mM Tris-HCl (pH 8.0), 100 mM NaCl, and 1 mM dithiothreitol).

Biophysical Characterization of RET-KD—Sucrose density gradient centrifugation of RET-KD was carried out on a 4–15% sucrose gradient in an SW40 rotor at 40,000 rpm for 16 h at 4 °C. RET-KD (0.5 mg/ml) was mixed with appropriate molecular mass standards and loaded onto the gradient solution. The gradient solutions were subsequently fractionated and analyzed by SDS-PAGE. Static light scattering analysis with concentrations of RET-KD between 0.5 and 1.0 mg/ml using a Zetasizer Nano (Malvern Instruments) was used to calculate a Debye plot, from which the molecular mass and second virial coefficient were derived according to the manufacturer's instructions.

Kinetic Parameters for RET-KD—Initial rates of phosphorylation by RET-KD were determined using a continuous ADP-coupled kinase assay with the random polymer poly(E_4Y) peptide as a substrate (44). The final assay mixture contained 100 mM Tris (pH 8.0), 10 mM $MgSO_4$, 2 mM phosphoenolpyruvate, 1 mM NADH, 20 μg/ml pyruvate kinase/lactate dehydrogenase (Roche Applied Science), and 25 μg/ml RET-KD in Buffer A. No ATP turnover was detectable without the addition of the poly(E_4Y) substrate, indicating that no RET-KD *trans*-phosphorylation or uncoupled ATPase activity occurred under these conditions. The K_m for the poly(E_4Y) peptide was determined using peptide concentrations of 0–16 mg/ml and a fixed ATP concentration of 500 μM. The K_m for ATP was determined using ATP concentrations of 0–600 μM and 4 mg/ml poly(E_4Y). The K_i for ZD6474 was determined by measuring the apparent K_m for ATP using the previous conditions in the presence of 300 nM ZD6474. The experiments were carried out in 96-well plates, and the NADH consumption was continuously read at 340 nm. Kinetic constants were determined by fitting data points to the Michaelis-Menten equation using the GraFit program (Erithacus Software). Each assay was performed at least three times with independent RET-KD preparations.

Western Blot Analysis—RET-KD-0P and RET-KD-P proteins were each resolved by SDS-PAGE and electroblotted onto polyvinylidene difluoride membranes. The blocked membranes were probed with anti-phosphotyrosine antibody 4G10 (Santa Cruz Biotechnology, Inc.) and incubated with horseradish peroxidase-conjugated anti-mouse antibody, and the Western blot was finally developed with the ECL system (Amersham Biosciences).

Mass Spectrometry—In-gel digests were performed, and phosphopeptides were mapped using an ABI 4700 matrix-assisted laser desorption ionization tandem time-of-flight proteomics analyzer (Applied Biosystems) and by on-line 4000 Q TRAP high pressure liquid chromatography as described by Craven *et al.* (45). Phosphorylation sites were identified primarily by independent data acquisition and were confirmed using the new software script MIDAS Workflow Designer developed by Applied Biosystems (46).

Phosphorylation of SPOT Peptide Arrays—Arrays of peptides based on the RET A-loop were synthesized on cellulose paper (5 × 10 cm) using a MultiPep synthesizer (Intavis AG) (47). The membranes were moistened with ethanol and then incubated for 2 h in 10 mM Tris (pH 8.0), 50 μM ATP, 100 μM $MgSO_4$, and 100 μg/ml bovine serum albumin. RET-KD (at a final concentration of 1.5 μg/ml) and 0.5 μl of [γ-^{32}P]ATP (10 μCi/ml) in the same buffer were subsequently added. After rocking overnight at 22 °C, the membranes were washed extensively with phosphate-buffered saline and then air-dried. Incorporation of ^{32}P into peptides on the membranes was assessed by film autoradiography with exposure times of 1–3 days.

Crystal Production—Crystals of RET-KD-P and RET-KD-0P were grown at 22 °C by vapor diffusion in sitting drops containing 1.5 μl of protein stock solution (3 mg/ml in Buffer A) mixed with 1 μl of reservoir solution (2.0 M sodium formate and 0.1 M sodium citrate (pH 5.5)). For screens with RET-KD-P, the protein stock solution also contained 2.5 mM ATP and 5 mM $MgCl_2$.

For the RET-KD-P inhibitor complexes, RET-KD was phosphorylated on glutathione-Sepharose beads as described above and washed with Buffer A. The beads were then incubated with a solution of inhibitor in Me_2SO for 2 h before being washed with Buffer A containing 1 mM EDTA and 1 mM sodium orthovanadate and then being cleaving with PreScission protease as described above. Crystals were grown at 16 °C by vapor diffusion in sitting drops. For PP1 (4-amino-5-(4-methylphenyl)-7-(*t*-butyl)pyrazolo[3,4-*d*]pyrimidine), the drops contained 1 μl of protein stock solution (1.5 mg/ml) and 1 μl of reservoir solution (2.8 M sodium formate, 0.1 M sodium acetate (pH 4.5), and 0.2 M lithium chloride); and for ZD6474 (*N*-(4-bromo-2-fluorophenyl)-6-methoxy-7-((1-methylpiperidin-4-yl)methoxy)quinazolin-4-amine), the drops contained 1.5 μl of protein stock solution (3 mg/ml) and 1 μl of reservoir solution (2.2 M sodium formate and 0.1 M sodium acetate (pH 4.5)). All crystals were harvested directly into the cryoprotectant *N*-paratone and flash-frozen in a dry nitrogen stream at −100 K.

Data Collection and Structure Solution—Data were collected (see Table 1) and processed with the program MOSFLM (48). The RET-KD-P structure was solved by molecular replacement using the program MOLREP (49) as implemented in the CCP4 Program Suite (50) using the fibroblast growth factor receptor 2 structure (Protein Data Bank code 1GJO) as a search model. After positioning the molecule, RESOLVE (51) was used in prime-and-switch mode to reduce phase bias. The structure was refined using REFMAC5 (52) and rebuilt using O (53) and Coot (54). Ligand libraries were generated with PRODRG (55). RET-KD-0P and the RET-KD-P complexes with PP1 and ZD6474 were solved and refined using a similar protocol, except that a partially refined model of RET-KD-P with the flexible loops deleted was used as the search model. Refinement statistics are given in Table 1, and coordinates have been deposited in the Protein Data Bank with codes 2IVS (RET-KD-0P), 2IVT (RET-KD-P), 2IVU (RET-KD-P·ZD6474), and 2IVV (RET-KD-P·PP1).

The RET-KD-P structures have continuous electron density from Gly^{700} (including five N-terminal vector-derived residues) to Ile^{711} and from Pro^{715} to Arg^{1012}, omitting the kinase insert domain residues 823–843, which are assumed to be disordered, and the molecules formed dimers related by a crystallographic 2-fold axis. RET-KD-0P has two molecules (referred to as A and B) related by a non-crystallographic 2-fold axis in the asymmetric unit, resulting in an AB dimer with an overall arrangement that is essentially the same as that found in the RET-KD-P

Structure and Inhibition of the RET Tyrosine Kinase Domain

TABLE 1

Data processing and refinement statistics

DL, Daresbury Laboratory; ESRF, European Synchrotron Radiation Facility; FMT, formate.

Data collection				
Protein	RET-KD-P	RET-KD-P	RET-KD-P	RET-KD-0P
Ligand	AMP	ZD6474	PP1	2′,3′-cAMP
Space group	C2	C2	C2	P21
Unit cell dimensions (Å)	$a = 72.13$, $b = 70.85$, $c = 78.92$; $\beta = 101.13°$	$a = 71.41$, $b = 71.42$, $c = 78.83$; $\beta = 101.23°$	$a = 72.13$, $b = 70.85$, $c = 78.92$; $\beta = 101.79°$	$a = 50.40$, $b = 80.22$, $c = 79.68$; $\beta = 100.09°$
Z_A	1	1	1	2
Resolution (Å)	2.6 (2.74-2.6)	2.5 (2.64-2.5)	2.25 (2.37-2.25)	2.0 (2.07-2.0)
Beamline	DL 14.2	In-house	In-house	ESRF ID14-4
Wavelength (Å)	0.9781	1.5418	1.5418	0.939
No. unique reflections	12,129	13,506	18,394	41,522
Average redundancy	3.6 (3.7)	3.7 (3.7)	3.9 (3.9)	4.0 (2.0)
Completeness	100 (100)	99.6 (99.6)	99.8 (99.8)	97.5 (80.6)
R_{merge} (%)	4.9 (13.4)	6.4 (16.5)	5.5 (19.5)	7.6 (24.7)
$I/\sigma(I)$	12.4 (5.1)	9.6 (4.6)	10.6 (3.9)	16 (10)
Wilson B	21.5	39.0	32.6	20.7
Refinement statistics				
Resolution (Å)[a]	50-2.6 (2.74-2.6)	50-2.5 (2.6-2.5)	25.7-2.25 (2.3-2.25)	50-2.00 (2.07-2.0)
No. reflections	11,547	12,835	17,476	39,256
R_{work} (%)	18.4	18.9	18.5	18.0
R_{free} (%)	24.9	24.8	23.7	23.0
No. atoms				
Protein	2236	2185	2158	4327
Ligand(s), water	5′-AMP, 23; FMT, 6; HOH, 62	ZD6474, 31; FMT, 6; HOH, 70	PP1, 21; FMT, 6; HOH, 122	2′,3′-cAMP, 44; FMT, 18; HOH, 262
Average B-factors (protein, ligands, water)	24, 31, 21	30, 31, 26	41, 36, 44	19 (A)/23 (B), 23, 27
r.m.s.d. from ideal values				
Bonds (Å)	0.017	0.015	0.017	0.015
Angles	1.69°	1.56°	1.54°	1.55°
Ramachandran plot (%)				
Allowed	90.4	92.8	92.2	91.8
Generously allowed	9.2	6.0	7.4	7.8
Disallowed	0.4	0.8	0.0	0.4

[a] Numbers in parentheses are values in the highest resolution shell.

structure (root mean square deviation (r.m.s.d.) of 0.5 Å for molecule A or B with RET-KD-P). Molecules A and B each have the same relative orientation of the N- and C-lobes (r.m.s.d. of 0.39 Å for 251 C-α atoms). Differences between molecules A and B are that, in molecule A, the N-terminal helix (helix αN) is only very poorly defined and is not included in the model, whereas the main chain for the A-loop is continuous with the Tyr[905] side chain clearly defined, not phosphorylated, and hydrogen-bonded to one water molecule. In molecule B, helix αN is present and clearly defined, but the A-loop residues 900–909 are disordered. Molecule A has been used in the comparisons in this study. No metal ions were located in any of the structures, despite the Mg^{2+}-ATP treatment used in the preparation of phosphorylated RET. Two very clear formate ions are common to all the structures. One bridges the NH_1 and NH_2 atoms of Arg[873] and the main chain nitrogen at residue 912, where it forms part of the surface of the ligand-binding pocket; and the other is at the interface between helix αN and the His[926] side chain of an adjacent protomer. Structural figures were made with PyMOL (DeLano Scientific, South San Francisco, CA).

RESULTS

Characterization of Recombinant RET-KD—As produced in Sf9 cells, purified RET-KD is partially phosphorylated, and we therefore treated these preparations with alkaline phosphatase to produce RET-KD-0P (Fig. 1*B*). To generate RET-KD-P and to ensure full phosphorylation, we incubated purified RET-KD with Mg^{2+}-ATP (Fig. 1*B*). Mass spectrometric analysis indicated that Tyr[900] and Tyr[905] were phos-

phorylated *in vitro*, as were Tyr[752], Tyr[826], Tyr[928], and Tyr[981], consistent with previous reports (14). Biophysical characterization of RET-KD by sucrose density gradient centrifugation and by gel filtration indicated an approximate molecular mass of 30 kDa, indicating that the protein was monomeric in solution (calculated molecular mass of 35.9 kDa); this was independently confirmed by static light scattering, where RET-KD had an apparent mass of 29 kDa.

We measured the enzyme kinetic constants for RET-KD-0P and RET-KD-P using a continuous coupled spectrophotometric assay to detect ADP generation (44). For these experiments, we used the synthetic peptide poly(E_4Y) as substrate and found that it could be efficiently phosphorylated with good saturation kinetics. We found a reproducible 3–4-fold increase in k_{cat} for the poly(E_4Y) substrate between RET-KD-0P and RET-KD-P (Table 2); the K_m value (and therefore, the affinity for poly(E_4Y)) was approximately the same in both cases, resulting in a 3–4-fold increase in overall catalytic efficiency (k_{cat}/K_m) upon phosphorylation of RET-KD. This is a markedly smaller difference than the 10–200-fold changes in catalytic efficiency found upon phosphorylation in other tyrosine kinases, *e.g.* the increase for insulin receptor kinase (IRK) with peptide substrate is 32-fold (56); it is comparable with the k_{cat}/K_m increase due to phosphorylation of VEGFR2 kinase using the poly(E_4Y) substrate (11-fold) (57), but without the parallel change in K_m. To confirm that the small kinetic differences in RET-KD were due to phosphorylation-dependent events, we performed similar measurements using the Y905F RET-KD mutant and found no change in the k_{cat} or K_m values following phosphorylation.
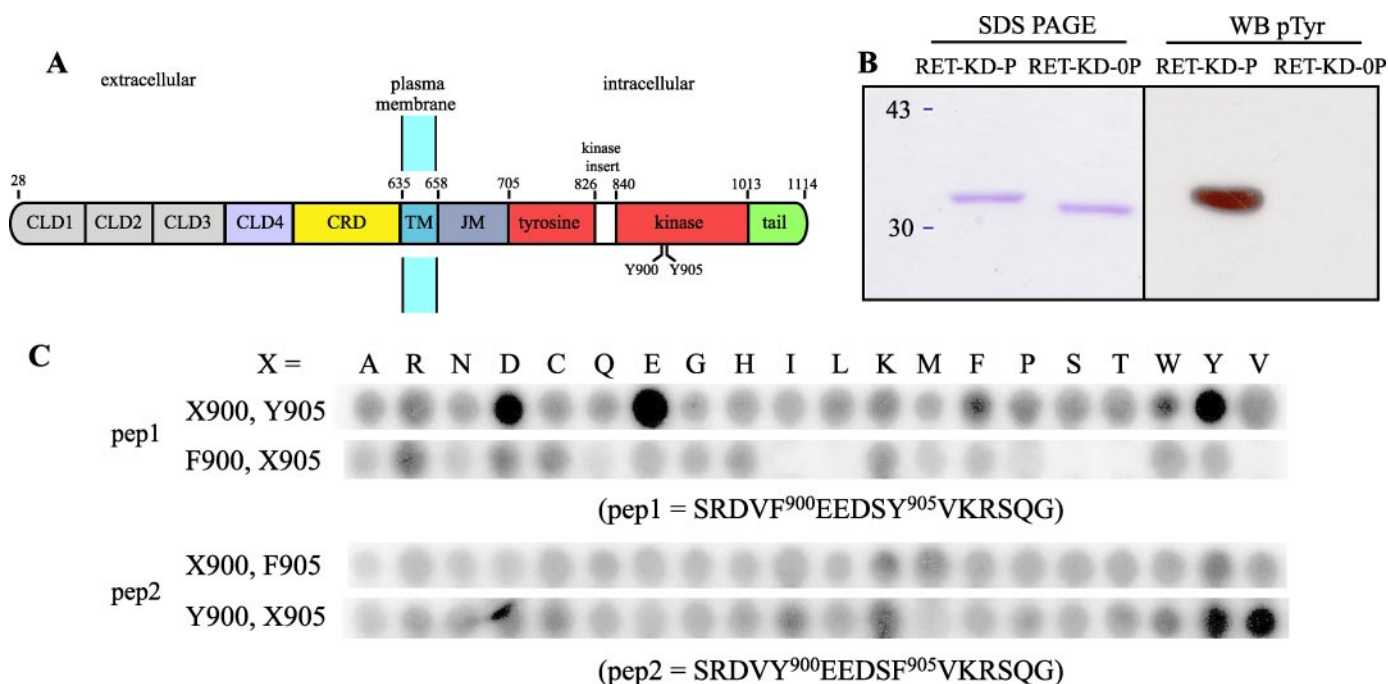
FIGURE 1. **Domain structure of RET and biochemical characterization of RET-KD.** *A*, the RET protein comprises an extracellular ligand-binding domain (residues 1–635) containing four cadherin-like domains (*CLD1–4*) with a single Ca^{2+}-binding site embedded between cadherin-like domains 2 and 3 (12), followed by a cysteine-rich domain (*CRD*), a single transmembrane region (*TM*), and RET-ICD (residues 666–1114) containing the protein-tyrosine kinase activity. RET-ICD comprises the juxtamembrane domain (*JM*); the core kinase domain (RET-KD), which contains an "insert domain," similar to a number of other RTKs; and a C-terminal tail. *B*, shown are a Coomassie Blue-stained SDS-polyacrylamide gel and an anti-phosphotyrosine Western blot (*WB*) of representative preparations of RET-KD-P (treated with Mg^{2+}-ATP) and RET-KD-0P (treated with alkaline phosphatase). *C*, the effects of systematic variation of residues 900 and 905 on phosphorylation of the RET A-loop-derived peptides were investigated. Shown are strips taken from SPOT membranes in which two peptides (peptides 1 (*pep1*) and peptide 2 (*pep2*)) based on the RET A-loop had residue 900 or 905 replaced with each of the 20 amino acids (shown above the strips), and their ability to act as RET-KD substrates was probed by treating the membranes with RET-KD-P and Mg^{2+}-[^{32}P]ATP and then assessing ^{32}P incorporation by autoradiography.

TABLE 2

Kinetic constants for RET-KD

Protein	K_m		k_{cat} for poly(E_4Y)	k_{cat}/K_m for poly(E_4Y)	K_i for ZD6474
	ATP	Poly(E_4Y)			
	μM	mg/ml	min^{-1}	ml/mg/min	nM
RET-KD-0P	446 ± 21	1.84 ± 0.48	55.0 ± 5.5	29.8	326 ± 90
RET-KD-P	429 ± 43	1.90 ± 0.84	207.0 ± 34.7	108.9	375 ± 27
Y905F RET-KD-0P	ND[a]	2.50 ± 0.45	79.8 ± 6.3	28.4	ND
Y905F RET-KD-P	ND	2.80 ± 0.90	78.5 ± 11.3	26.1	ND
RET-JM-KD-0P	ND	2.12 ± 0.43	40.1 ± 2.6	18.9	ND
RET-JM-KD-P	ND	2.47 ± 0.38	121.0 ± 5.0	49.0	ND
RET-ICD-0P	157 ± 25	2.88 ± 0.64	61.4 ± 6.2	21.3	ND
RET-ICD-P	212 ± 18	4.13 ± 0.62	201.4 ± 15.8	48.8	ND

[a] ND, not determined.

We concluded that Tyr[905] is not required for RET catalytic activity *in vitro* and that only a small catalytic enhancement occurs upon RET-KD autophosphorylation.

To investigate whether an additional regulatory mechanism exists outside the kinase domain, we prepared two additional baculoviruses and recombinant proteins: RET-JM-KD (residues 666–1013), including the juxtamembrane domain, and RET-ICD (residues 666–1114), encompassing the entire intracellular portion of RET. Again, we assayed these proteins in the phosphorylated and non-phosphorylated states and found the same 3–4-fold increase in k_{cat} and no significant lowering of the K_m upon phosphorylation. Thus, the *in vitro* activity of soluble RET-ICD by only modestly enhanced by phosphorylation, and no *cis*-inhibitory mechanism was evident even within the entire soluble intracellular domain, unlike the kinases present in other receptors (58).

To attempt to distinguish between the roles of Tyr[900] and Tyr[905] in activation and substrate recognition, we prepared peptide arrays based on the RET A-loop. These synthetic RET substrates were attached to cellulose membranes by SPOT synthesis (59). The peptides SRDVF[900]EEDSY[905]VKRSQG (peptide 1) and SRDVY[900]EEDSF[905]VKRSQG (peptide 2), each with a single tyrosine site, were systematically varied at positions 900 and 905. Phosphorylation of peptide 1 was barely detectable unless residue 900 was Tyr, Glu, or Asp (Fig. 1*C*). Therefore, the presence of only Tyr[905] in the peptide was insufficient to make it a good RET substrate, but rather both Tyr[905] and Tyr[900] or a phospho-Tyr[900] mimetic was required. In contrast, peptide 2 was efficiently phosphorylated only when residue 905 was Tyr or Val, but this effect could not be mimicked by an acidic residue.
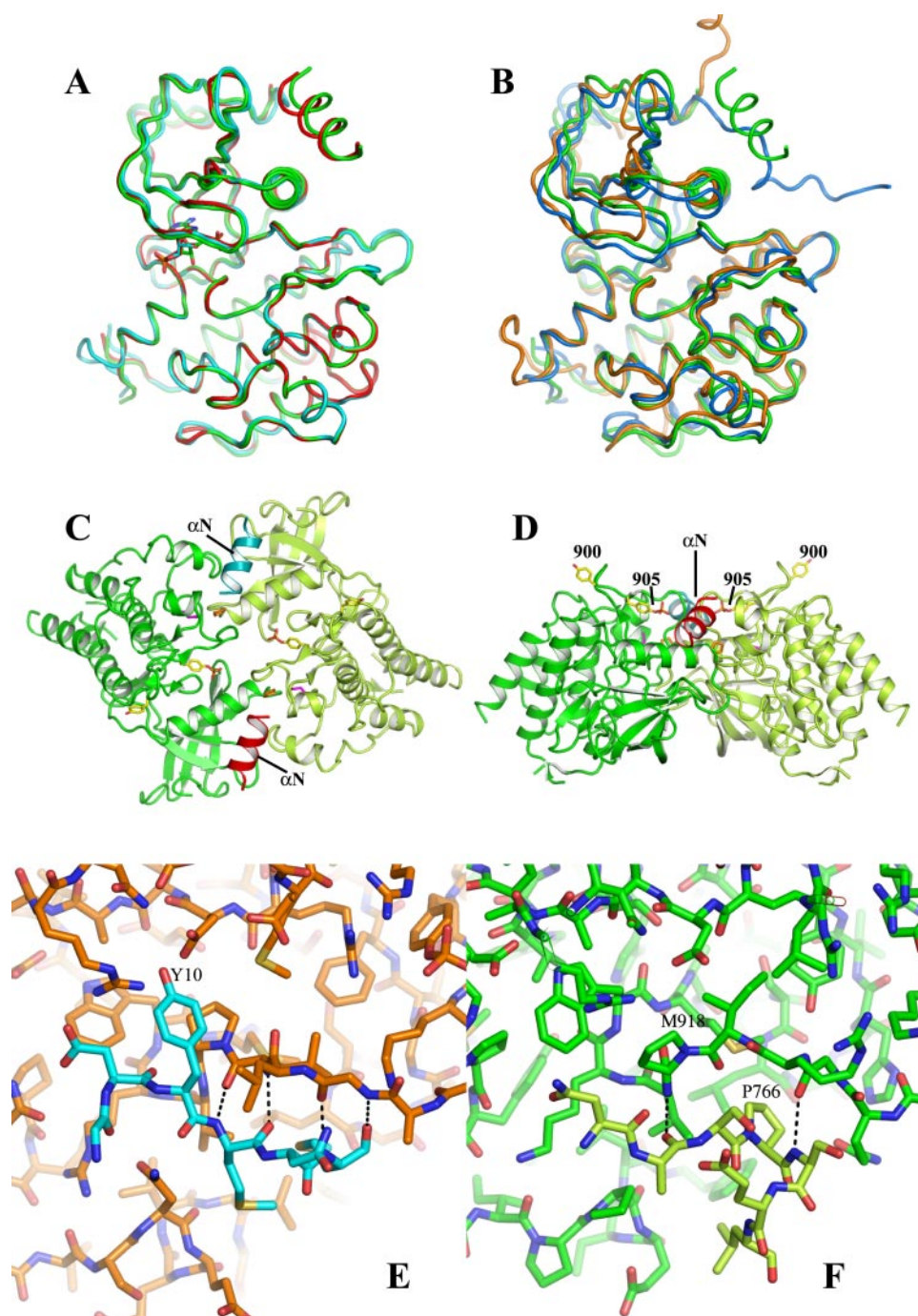
FIGURE 2. **RET kinase structures.** *A*, RET-KD-P (*green*) and RET-KD-0P (*cyan* for molecule A and *red* for molecule B) structures superimposed using the C-lobe C-α atoms. The bound nucleotides are shown as sticks. *B*, RET-KD-P (*green*), activated IRK (Protein Data Bank code 1IR3; *orange*), and Kit (Protein Data Bank code 1PKG; *blue*) structures superimposed using equivalent C-lobe C-α atoms. *C* and *D*, orthogonal views of the *trans*-inhibited RET-KD dimer with molecule A in *green* and molecule B in *light green*. Their N-terminal helices are *red* and *cyan*, respectively. Side chain sticks are shown for Tyr[900] and Tyr[905] (*orange*), Met[918] (*magenta*), and Pro[766] (*orange*). *E*, main chain hydrogen bond contacts in the complex structure (Protein Data Bank code 1IR3) between IRK (*orange*) and substrate peptide (*cyan*). *F*, main chain hydrogen bond contacts in RET-KD between the Met[918] pocket of molecule A (*green*) and Pro[766] of molecule B (*light green*).

C-α atoms of 0.49 Å (Fig. 2*A*), despite their having adopted two different crystal lattices. Structural alignment using the Secondary Structure Matching server (www.e-bi.ac.uk/msd-srv/ssm/) showed the closest similarity to active kinase forms, including fibroblast growth factor receptor 2 (Protein Data Bank code 1OEC; r.m.s.d. of 0.87 Å), Kit (Protein Data Bank code 1PKG; r.m.s.d. of 1.07 Å), ACK1 (Protein Data Bank code 1U46; r.m.s.d. of 0.81 Å), and IRK (Protein Data Bank code 1IR3; r.m.s.d. of 1.22Å) (Fig. 2*B*). A notable feature of the RET-KD structure is the presence of residues 705–711 of the RET juxtamembrane domain. In RET-KD-P, these residues form part of an N-terminal helix (helix αN) that connects to the β1 strand of the kinase domain via loop 712–714, for which no electron density was observed. Helix αN packs against and tethers the functionally important helix αC through apolar contacts around Phe[709] and Phe[776]. A similar N-terminal helix is found in the autoinhibited c-Met kinase structure (60).

In both RET-KD-0P and RET-KD-P structures, the A-loop is ordered. In the crystals of RET-KD-P, Tyr[905] is clearly phosphorylated, and Tyr[900] is not; in RET-KD-0P, Tyr[905] is hydrogen-bonded to one water molecule, and the side chain of Tyr[900] is disordered. Because mass spectrometric results showed that Tyr[900] is phosphorylated, phospho-Tyr[900] may be labile to water-mediated hydrolysis, which would be favored by the high solvent accessibility of Tyr[900] and the absence of a binding pocket for this residue. A similar situation was observed in the VEGFR2 kinase domain structure, where Tyr[1054], the structural equivalent of Tyr[900], is phosphorylated in solution, but not in crystals (61). In contrast, phospho-Tyr[905] is protected through interaction with a group of basic side chains; three residues, Arg[770], Arg[897], and Lys[907], contact phospho-Tyr[905], in contrast to the single tether found in other RTKs, *e.g.* Arg[1155] in the activated IRK structure (which is structurally equivalent to Arg[897] in RET). The position of the Arg[897] side chain is the same in the RET-KD-P and RET-KD-0P

Structure of RET-KD—RET-KD adopts a characteristic protein kinase fold consisting of a smaller N-lobe (residues 713–805) and a larger C-lobe (residues 812–1013) connected by a hinge/linker (residues 806–811). The relative orientation of the N- and C-lobes is essentially the same in the phosphorylated and non-phosphorylated RET forms, with an r.m.s.d. for 268

structures and is stabilized by interaction with the carbonyl oxygen at position 894, but in RET-KD-0P, the side chains of Arg[770] and Lys[907] are disordered. The observed k_{cat} enhancement could be explained by phospho-Tyr[905] organizing this cluster of side chains. The conserved salt bridge between Lys[758] and Glu[775] from helix αC, equivalent to that found in most activated RTKs, is formed in both structures, although the torsion angles within the two side chains are slightly different. The relative position of the N- and C-lobes is further stabilized by a salt bridge between Arg[912] and Asp[771], which is not generally present in RTKs. The global RET-KD conformation is thus independent of the phosphorylation state of the A-loop and suggests that the A-loop exhibits no major autoinhibitory effect on binding of either ATP or substrate, consistent with our kinetic data. RET-KD is basic (calculated pI 8.6), but the majority of the accessible acidic residues are clustered within the A-loop. Positive charge found in the vicinity of the substrate-binding site should favor the acidic A-loop as a substrate and may contribute to the efficiency with which RET phosphorylates poly(E_4Y) peptides.

A Possible trans-Inhibited RET-KD Dimer—Although apparently monomeric in solution, as shown by sucrose density gradient ultracentrifugation and static light scattering, RET-KD adopts two independent crystal forms that each contain an identical head-to-tail dimer generated by either non-crystallographic (RET-KD-0P, P2$_1$) or crystallographic (RET-KD-P, C2) symmetry, with ~1090 Å^2 of buried surface/monomer (Fig. 2, *C* and *D*). We also observed the same dimer in the preliminary crystal structure of RET-JM-KD, which includes both the juxtamembrane and kinase domains, suggesting a strong preference for this particular arrangement.[5] The first contact area within the dimer involves N[763]ASPS[767], prior to helix C interacting with the P+3 pocket and specifically Met[918]. Residues 763–767 are in an extended conformation that masks the substrate-binding site of the second molecule in a manner reminiscent of both the peptide-bound form of triphosphorylated IRK (Protein Data Bank code 1IR3) and the interaction of the juxtamembrane domain of c-Kit in the product complex (Protein Data Bank code 1PKG) with a second molecule. In both triphosphorylated IRK and c-Kit, the main chain nitrogen and oxygen of the P+1 residue form hydrogen bonds with main chain atoms in the C-terminal segment of the A-loop (Fig. 2*E*). There are no directly equivalent hydrogen bonds in RET, although there are main chain contacts between O-764 and N-915 and between N-766 and O-911 and a central van der Waals contact from Pro[766] of one protomer to Met[918] within an apolar cleft formed by the P+1 loop of the other protomer (discussed below) (Fig. 2*F*). A second, adjacent contact area in the dimer involves helix αN interacting with the side chains of Phe[924] and Phe[961] and (via a formate ion) and with Gln[910] and His[926]. This dimer structure represents a *trans*-inhibited state despite being formed by molecules in an active conformation.

Small Molecule Ligands—We have determined the structures of RET-KD-P with AMP, PP1, and ZD6474 in the ATP pocket and of RET-KD-0P with 2′,3′-cAMP. AMP binds in

a manner similar to ADP/ATP observed in other RTKs. Although we might have expected a product complex to contain ADP, there is no electron density for a β-phosphate, and there does not appear to be space to accommodate it.

Co-crystallization of RET-KD-P with ZD6474 and PP1 led to well ordered ligands in the ATP-binding site (Fig. 3, *A* and *B*). Compared with the AMP complex, the site accommodated the larger PP1 and ZD6474 by adjusting the nucleotide-binding loop and a bulging of the linker strand 804–808. This is most obvious when RET-KD-P·ZD6474 is compared with RET-KD-P·AMP; the α-carbon atoms of residue 734 in the two structures are 1.57 Å apart, and the side chain of Phe[735] is not seen in the ZD6474 complex, whereas in the AMP complex, it packs against the aliphatic part of the Lys[758] side chain. Small movements of residues 804–806 produced a different conformation for the side chain of Glu[805], where it cannot form a hydrogen bond with Lys[889]. PP1 forms the two canonical nucleotide hydrogen bonds with the linker region (Fig. 3*D*), whereas the quinazoline moiety of ZD6474 can mimic only one, the equivalent of N1–807N in the AMP complex (Fig. 3*C*). Other contacts between RET-KD and the inhibitors are shown in Fig. 3 (*C* and *D*). The methylphenyl group of PP1 and the bromofluorophenyl group of ZD6474 each occupy the small hydrophobic cavity at the back of the ATP site, which has Val[804] in the gatekeeper (62, 63) position (Fig. 3, *E–G*). In RET-KD-P·ZD6474, this cavity also encloses one water molecule that bridges the side chain of Glu[775] and the main chain nitrogen atom of Asp[892].

DISCUSSION

In the majority of previously characterized RTK-KD structures, A-loop phosphorylation stimulates kinase activity by causing structural changes that relieve *cis*-autoinhibition. The non-phosphorylated basal states of many RTKs have low catalytic activity because of a suboptimal A-loop conformation that interferes with either the ATP- or substrate-binding sites (reviewed, for example, by Schlessinger (64)). In contrast, we have found that the A-loop phosphorylation state of RET-KD made no substantial difference to the three-dimensional structure and only modestly affected the level of its catalytic activity. Other tyrosine kinases with active A-loop conformations in their non-phosphorylated states include EGFR kinase (65) and the non-receptor tyrosine kinase ACK1 (66). For EGFR, ligand-dependent allosteric changes are required for receptor activation (67). Similar to ACK1, phospho-Tyr[905] of RET-KD stabilizes a surrounding constellation of basic residues, rather than the single one found in most tyrosine kinases. A mechanism similar to that proposed for ACK1, in which a favorable electrostatic environment promotes an increased rate of phosphoryl transfer, may explain the increased catalytic efficiency of RET-KD-P.

It is not yet clear whether the essential role of Tyr[905] in constitutive (MEN2A and PTC) and transient (GDNF-dependent) RET dimers can be explained simply by the modest increase in catalytic rates of RET-KD. We have shown that, *in vitro*, Tyr[905] and Tyr[900] (or a phosphomimetic at position 900) are required for efficient phosphorylation of the RET-KD A-loop peptide, but it is possible that further functions of phospho-Tyr[905] remain to be found, such as promoting an active RET dimer or
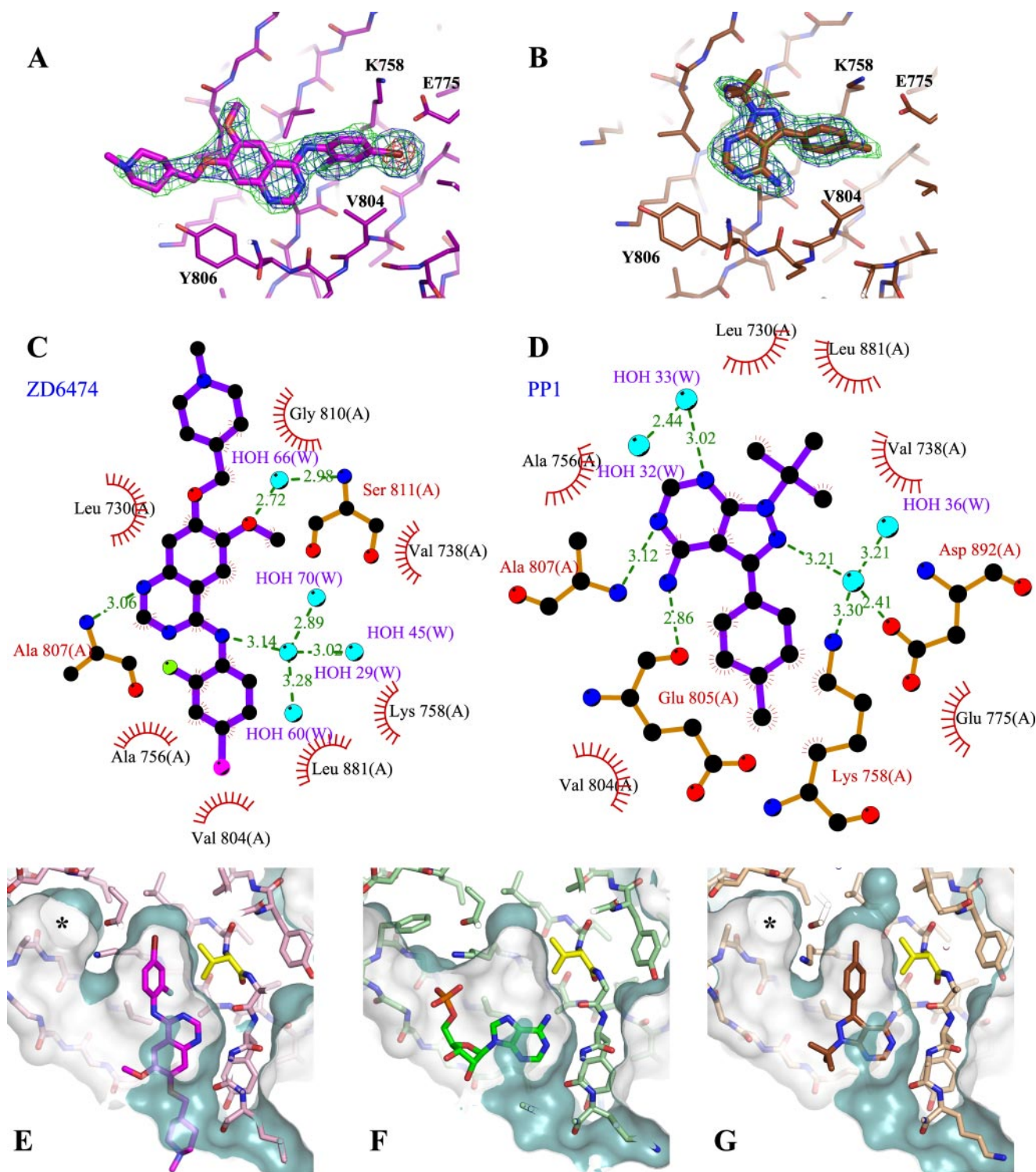
[5] S. Kjær, unpublished data.

FIGURE 3. **Ligand-binding sites.** Electron density maps around ZD6474 (*A*) and PP1 (*B*) show REFMAC-calculated electron density maps with $2mF_o − DF_c$ contoured at 1σ in *green* and $mF_o − DF_c$ contoured at 3σ in *blue* and (in *A*) contoured at 8σ in *red*. *C* and *D* are Ligplot (79) schematic diagrams of ZD6474 and PP1 contacts with RET. Water molecules (*W*) are shown in *cyan*. *E–G* show molecular surfaces of the ligand-binding pockets in RET-KD-P, with the solvent side of the surface *white* and the inside of the surface *blue-green*. Ligands are shown in stick form, with carbon atoms *magenta* for ZD6474 (*E*), *green* for AMP (*F*), and *brown* for PP1 (*G*). The Val[804] side chain is highlighted in *yellow*. The pocket with access that is controlled by Val[804] is in the center of each diagram; a second apparent pocket (*) in *E* and *G* is the result of the Phe[735] side chain being disordered in these two complexes.

prolonging RET activation to allow other phosphotyrosine sites to engage with adaptor molecules. In contrast, highly transforming MEN2B mutants do not require Tyr[905] phosphorylation, possibly because cell transformation can occur in the absence of detectable RET dimerization. However, M918T RET

can be further activated by an additional MEN2A mutation (C634R) and stimulation by GDNF (68) or PTC fusion (69), suggesting that dimerization is important for maximal activation.

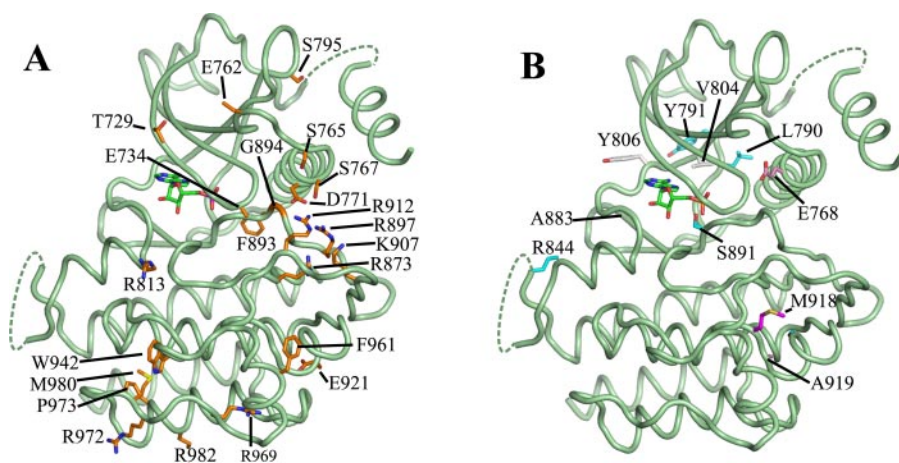Our results show no *cis*-inhibitory mechanism within the

FIGURE 4. **Mapping of disease-linked mutations on the RET kinase structure.** The backbone schematic of RET-KD is shown in *green*, with the link to the N-terminal helix and the kinase insert domain indicated by *dashed lines*. The side chains of wild-type RET-KD are shown, and the bound nucleotide is indicated in stick form. *A*, inactivating mutation sites in RET-KD found in familial and/or sporadic Hirschsprung disease (18). Carbon atoms of the side chains are colored *orange* to mark mutation sites. The effects of some of these mutations can be rationalized from the structure, *e.g.* W942C in the conserved kinase core and F961L in a hydrophobic region would both be expected to destabilize the structure. Mutations of essential residues, such as R873Q in the kinase RD motif and F893L and G894S in the invariant DFG motif, will lower or abolish catalytic activity. Mutations of basic side chains that coordinate phospho-Tyr[905], including R897Q and K907E, will perturb the optimal active kinase conformation and lower affinity for phosphotyrosine. Asp[771] and Arg[912] form a salt bridge that links the N- and C-lobes, stabilizing the active conformation. E734K at the tip of the conformationally sensitive nucleotide-binding loop mutation may perturb its interaction with Arg[912], although this is not structurally critical, as Arg[912] is disordered in RET-KD-P. Both S765P and S767R, in positions preceding helix C, may affect helix C orientation. Other mutations, including E762Q and R982C, are solvent-accessible and have no obvious detrimental impact on the RET-KD structure. *B*, activating mutation sites in RET-KD identified in MTC, MEN2A, and MEN2B. Carbon atoms of the side chains are colored *magenta* for M918T, the predominant MEN2B mutant; *pink* for E768D/A919P and *white* for V804M/Y806C, two paired mutations where there is synergy; and *cyan* for L790F, Y791F, S891A, and R844L.

niscent of, but distinct from, the recently described allosteric activation of EGFR by formation of an asymmetric dimer (71). An alternative inhibitory mechanism might be that, in cells, *trans*-inhibition of RET is overcome during the process of signaling complex assembly and recruitment to lipid rafts. Different partner proteins are known to associate with RET depending on its localization (72), and heterotypic repressive interaction with other membrane-localized partners is a possibility.

Both PP1 and ZD6474 inhibit the active conformation of RET-KD and can therefore target both phosphorylated and non-phosphorylated forms. This is supported by our K_i values for ZD6474 (Table 2), which suggest that it is equally potent toward both RET-KD-P and RET-KD-0P. Functional groups from PP1 and ZD6474 utilize a pocket with access that is controlled by the gatekeeper residue Val[804], a position that controls kinase sensitivity to several structurally unrelated types of inhibitor (73). In BCR-ABL, the equivalent residue (Thr[315]) forms a hydrogen bond with Gleevec and is small enough to allow access to the pocket, but mutations of larger side chains lead to Gleevec-resistant chromic myeloid leukemia (74). Although Val[804] of RET cannot form hydrogen bonds with the inhibitors, the size of the side chain at this position controls access to the pocket, explaining why Val[804] mutants with the bulkier leucine or methionine side chains that are found in MTC and MEN2 cases are not inhibited by ZD6474 (42, 75). As with other kinases (73), mutation of Val[804] to alanine or glycine renders RET even more sensitive to inhibition by ZD6474 and PP1 (42), possibly because of greater plasticity in the pocket; however, such small side chains are not generally found as the gatekeeper in wild-type kinases (63). The identity of the gatekeeper shows why ZD6474 is able to selectively inhibit EGFR, VEGFR2, and RET, but not IRK (41), in which the larger methionine side chain occupies the gatekeeper position. Other residues in contact with ZD6474 (Fig. 3C) are conserved in VEGFR2 and EGFR. These residues are also conserved within fibroblast growth factor receptor 1, which is less potently inhibited by ZD6474 (IC$_{50}$ > 1 μM) (41). Here, variations in residues further removed from the ligand may lower the nucleotide-binding loop flexibility required to accommodate the inhibitor; in particular, the equivalents to RET-KD Thr[729] and Glu[734] are proline and cysteine in fibroblast growth factor receptor 1.

isolated RET-ICD and only a low activation threshold, which together could lead to uncontrolled intracellular phosphorylation events. However, in cells, RET signaling requires interaction with ligand and co-receptor and subsequent Tyr[905] autophosphorylation. This suggests that RET kinase activity must be regulated in a manner that is not apparent from studying RET-KD in solution and does not involve the juxtamembrane domain, in contrast to the autoinhibition of c-Kit (70). We therefore considered whether RET might be *trans*-inhibited and whether there is an allosteric component to RET activation. The crystallographic RET dimer described here has mutually occluded substrate-binding sites (Fig. 2D) and persists in both RET-KD crystal forms and in RET-JM-KD; it may therefore represent a biologically relevant *trans*-inhibited state of RET. Several transforming mutations map to positions close to the dimer contacts, including M918T, P766S, and E768D/A919P (see below), and may destabilize this dimer. If this dimer were to define an inhibited form of RET, a large conformational change would be required to relieve the *trans*-inhibition, and it may be driven by interaction with GDNF/GFRα1. RET/PTC dimers are constitutively active and therefore must have accessible substrate-binding pockets. These molecules lack the juxtamembrane domain including helix αN, which forms an integral part of the RET dimer interface. It is conceivable that, without the juxtamembrane domain, RET/PTC cannot form the *trans*-inhibited dimer, but is still capable of forming an active RET dimer. Further investigation of the biological relevance of the *trans*-inhibited dimer is merited, through directed mutagenesis in a full-length RET context. This model is remi-

Familial and sporadic missense mutations in RET-KD resulting in Hirschsprung disease are generally inactivating, and in structural terms, they fall roughly into three categories: those that directly affect essential kinase residues, those that lead to charge

reversals or loss of charged residues, and those that remove or introduce bulky hydrophobic residues (Fig. 4*A*). Several germ line and sporadic activating mutations reported for MTC and MEN2B phenotypes lie within RET-KD (Fig. 4*B*); they are harder to rationalize than the Hirschsprung disease mutations because they have multiple effects on RET function. The best studied example is the germ line mutation M918T found in 95% of MEN2B patients. As with the equivalent mutation in the RON (76) and Met (77) receptors, M918T has an unexpectedly large effect on RET function. It both abrogates the requirement for A-loop phosphorylation and facilitates phosphorylation of novel substrates such as STAT3 (29). Structurally, Met^{918} forms part of the P+3 pocket, and replacing it with threonine may not only alter the shape of the pocket, but also lower the flexibility of the P+1 loop. In the dimer we have described, Met^{918} in the P+3 pocket of one molecule contacts Pro^{766} of the second molecule. Replacement of the Met^{918} side chain with the shorter threonine may weaken the *trans*-inhibitory dimer interaction, facilitating formation of an active dimer, as may the rarer P766S mutation (78). Inhibitory dimer formation likewise brings Glu^{768} and Ala^{919} into closer proximity than would be predicted from an isolated kinase domain structure, and this may underlie the synergistic effect of the separate low transforming mutations E768D and A919P in the highly transforming E768D/A919P double mutation (25). Other mutations, including A883F (between the N- and C-lobes), L790F and Y791F (in the N-lobe), and V804M/Y806C (within the linker), are likely to affect interlobe flexibility, which may favor maintenance of an active RET-KD conformation.

CONCLUSION

Crystals of both phosphorylated and non-phosphorylated forms of RET-KD contain molecules with the structural characteristics of an active tyrosine kinase. Enzyme kinetic parameters show only very modest catalytic enhancement resulting from phosphorylation, and we have concluded that RET does not employ *cis*-inhibition to control inappropriate activity. In crystals, RET-KD molecules associate as dimers with mutually occluded binding sites. Several transforming mutations map close to the dimer interface, suggesting that they destabilize this arrangement of RET-KD. This dimer persists in both phosphorylated and non-phosphorylated RET-KD and in the longer RET-JM-KD, suggesting that it may be a preferred association that defines a *trans*-inhibited RET dimer. Structures of RET-KD with the inhibitors PP1 and ZD6474 demonstrate the mode of binding and the basis for inhibitor resistance in some RET-KD mutants.

REFERENCES

1. Takahashi, M., Ritz, J., and Cooper, G. M. (1985) *Cell* **42,** 581–588
2. Takahashi, M., Buma, Y., Iwamoto, T., Inaguma, Y., Ikeda, H., and Hiai, H. (1988) *Oncogene* **3,** 571–578
3. Trupp, M., Arenas, E., Fainzilber, M., Nilsson, A. S., Sieber, B. A., Grigoriou, M., Kilkenny, C., Salazar-Grueso, E., Pachnis, V., Arumäe, U., Sariola, H., Saarma, M., and Ibáñez, C. F. (1996) *Nature* **381,** 785–789
4. Treanor, J. J., Goodman, L., de Sauvage, F., Stone, D. M., Poulsen, K. T., Beck, C. D., Gray, C., Armanini, M. P., Pollock, R. A., Hefti, F., Phillips, H. S., Goddard, A., Moore, M. W., Buj-Bello, A., Davies, A. M., Asai, N., Takahashi, M., Vandlen, R., Henderson, C. E., and Rosenthal, A. (1996) *Nature* **382,** 80–83
5. Durbec, P., Marcos-Gutierrez, C. V., Kilkenny, C., Grigoriou, M., Wartiowaara, K., Suvanto, P., Smith, D., Ponder, B., Costantini, F., Saarma, M., Sariola, H., and Pachnis, V. (1996) *Nature* **381,** 789–793
6. Sariola, H., and Saarma, M. (2003) *J. Cell Sci.* **116,** 3855–3862
7. Jing, S., Wen, D., Yu, Y., Holst, P. L., Luo, Y., Fang, M., Tamir, R., Antonio, L., Hu, Z., Cupples, R., Louis, J. C., Hu, S., Altrock, B. W., and Fox, G. M. (1996) *Cell* **85,** 1113–1124
8. Schuchardt, A., D'Agati, V., Larsson-Blomberg, L., Costantini, F., and Pachnis, V. (1994) *Nature* **367,** 380–383
9. Costantini, F., and Shakya, R. (2006) *BioEssays* **28,** 117–127
10. Airaksinen, M. S., and Saarma, M. (2002) *Nat. Rev. Neurosci.* **3,** 383–394
11. Arighi, E., Borrello, M. G., and Sariola, H. (2005) *Cytokine Growth Factor Rev.* **16,** 441–467
12. Anders, J., Kjær, S., and Ibáñez, C. F. (2001) *J. Biol. Chem.* **276,** 35808–35817
13. Nozaki, C., Asai, N., Murakami, H., Iwashita, T., Iwata, Y., Horibe, K., Klein, R. D., Rosenthal, A., and Takahashi, M. (1998) *Oncogene* **16,** 293–299
14. Kawamoto, Y., Takeda, K., Okuno, Y., Yamakawa, Y., Ito, Y., Taguchi, R., Kato, M., Suzuki, H., Takahashi, M., and Nakashima, I. (2004) *J. Biol. Chem.* **279,** 14213–14224
15. Besset, V., Scott, R. P., and Ibáñez, C. F. (2000) *J. Biol. Chem.* **275,** 39159–39166
16. Coulpier, M., Anders, J., and Ibáñez, C. F. (2002) *J. Biol. Chem.* **277,** 1991–1999
17. Santoro, M., Melillo, R. M., Carlomagno, F., Vecchio, G., and Fusco, A. (2004) *Endocrinology* **145,** 5448–5451
18. Kashuk, C. S., Stone, E. A., Grice, E. A., Portnoy, M. E., Green, E. D., Sidow, A., Chakravarti, A., and McCallion, A. S. (2005) *Proc. Natl. Acad. Sci. U. S. A.* **102,** 8949–8954
19. Chappuis-Flament, S., Pasini, A., De Vita, G., Segouffin-Cariou, C., Fusco, A., Attie, T., Lenoir, G. M., Santoro, M., and Billaud, M. (1998) *Oncogene* **17,** 2851–2861
20. Kjær, S., and Ibáñez, C. F. (2003) *Hum. Mol. Genet.* **12,** 2133–2144
21. Carlomagno, F., De Vita, G., Berlingieri, M. T., de Franciscis, V., Melillo, R. M., Colantuoni, V., Kraus, M. H., Di Fiore, P. P., Fusco, A., and Santoro, M. (1996) *EMBO J.* **15,** 2717–2725
22. Iwashita, T., Murakami, H., Asai, N., and Takahashi, M. (1996) *Hum. Mol. Genet.* **5,** 1577–1580
23. Geneste, O., Bidaud, C., De Vita, G., Hofstra, R. M., Tartare-Deckert, S., Buys, C. H., Lenoir, G. M., Santoro, M., and Billaud, M. (1999) *Hum. Mol. Genet.* **8,** 1989–1999
24. Iwashita, T., Asai, N., Murakami, H., Matsuyama, M., and Takahashi, M. (1996) *Oncogene* **12,** 481–487
25. Iwashita, T., Kato, M., Murakami, H., Asai, N., Ishiguro, Y., Ito, S., Iwata, Y., Kawai, K., Asai, M., Kurokawa, K., Kajita, H., and Takahashi, M. (1999) *Oncogene* **18,** 3919–3922
26. Iwashita, T., Murakami, H., Kurokawa, K., Kawai, K., Miyauchi, A., Futami, H., Qiao, S., Ichihara, M., and Takahashi, M. (2000) *Biochem. Biophys. Res. Commun.* **268,** 804–808
27. Takahashi, M., Asai, N., Iwashita, T., Murakami, H., and Ito, S. (1998) *J. Intern. Med.* **243,** 509–513
28. Miše, N., Drosten, M., Racek, T., Tannapfel, A., and Pützer, B. M. (2006) *Oncogene*, in press
29. Yuan, Z. L., Guan, Y. J., Wang, L., Wei, W., Kane, A. B., and Chin, Y. E. (1999) *Mol. Cell. Biol.* **24,** 9390–9400
30. Schuringa, J. J., Wojtachnio, K., Hagens, W., Vellenga, E., Buys, C. H., Hofstra, R., and Kruijer, W. (2001) *Oncogene* **20,** 5350–5358
31. Jhiang, S. M. (2000) *Oncogene* **19,** 5590–5597
32. Buckwalter, T. L., Venkateswaran, A., Lavender, M., La Perle, K. M., Cho, J. Y., Robinson, M. L., and Jhiang, S. M. (2002) *Oncogene* **21,** 8166–8172
33. Blume-Jensen, P., and Hunter, T. (2001) *Nature* **411,** 355–365
34. Carlomagno, F., and Santoro, M. (2005) *Curr. Med. Chem.* **12,** 1773–1781

35. Vidal, M., Wells, S., Ryan, A., and Cagan, R. (2005) *Cancer Res.* **65,** 3538–3541

36. Drosten, M., Stiewe, T., and Pützer, B. M. (2003) *Hum. Gene Ther.* **14,** 971–982

37. Noble, M. E., Endicott, J. A., and Johnson, L. N. (2004) *Science* **303,** 1800–1805

38. Hubbard, S. R. (2002) *Curr. Opin. Struct. Biol.* **12,** 735–741

39. Waltenberger, J., Uecker, A., Kroll, J., Frank, H., Mayr, U., Bjorge, J. D., Fujita, D., Gazit, A., Hombach, V., Levitzki, A., and Böhmer, F. D. (1999) *Circ. Res.* **85,** 12–22

40. Carlomagno, F., Vitagliano, D., Guida, T., Napolitano, M., Vecchio, G., Fusco, A., Gazit, A., Levitzki, A., and Santoro, M. (2002) *Cancer Res.* **62,** 1077–1082

41. Ryan, A. J., and Wedge, S. R. (2005) *Br. J. Cancer* **92,** Suppl. 1, S6–S13

42. Carlomagno, F., Guida, T., Anaganti, S., Vecchio, G., Fusco, A., Ryan, A. J., Billaud, M., and Santoro, M. (2004) *Oncogene* **23,** 6056–6063

43. Daub, H., Specht, K., and Ullrich, A. (2004) *Nat. Rev. Drug Discov.* **3,** 1001–1010

44. Barker, S. C., Kassel, D. B., Weigl, D., Huang, X., Luther, M. A., and Knight, W. B. (1995) *Biochemistry* **34,** 14843–14851

45. Craven, R. A., Stanley, A. J., Hanrahan, S., Dods, J., Unwin, R. D., Totty, N., Harnden, P., Eardley, I., Selby, P. J., and Banks, R. E. (2006) *Proteomics* **6,** 3880–3893

46. Unwin, R. D., Griffiths, J. R., Leverentz, M. K., Grallert, A., Hagan, I. M., and Whetton, A. D. (2005) *Mol. Cell. Proteomics* **4,** 1134–1144

47. Frank, R., and Overwin, H. (1996) *Methods Mol. Biol.* **66,** 149–169

48. Leslie, A. G. W. (1992) *Joint CCP4 and ESF-EAMCB Newsletter on Protein Crystallography*, No. 26, Daresbury Laboratories, Warrington, UK

49. Vagin, A., and Teplyakov, A. (1997) *J. Appl. Crystallogr.* **30,** 1022–1025

50. Collaborative Computational Project, N. (1994) *Acta Crystallogr. Sect. D Biol. Crystallogr.* **50,** 760–763

51. Terwilliger, T. C. (2000) *Acta Crystallogr. Sect. D Biol. Crystallogr.* **56,** 965–972

52. Murshudov, G. N., Vagin, A. A., and Dodson, E. J. (1997) *Acta Crystallogr. Sect. D Biol. Crystallogr.* **53,** 240–255

53. Jones, T. A., Zou, J.-Y., Cowan, S. W., and Kjeldgaard, M. (1991) *Acta Crystallogr. Sect. A* **47,** 110–119

54. Emsley, P., and Cowtan, K. (2004) *Acta Crystallogr. Sect. D Biol. Crystallogr.* **60,** 2126–2132

55. Schuttelkopf, A. W., and van Aalten, D. M. (2004) *Acta Crystallogr. Sect. D Biol. Crystallogr.* **60,** 1355–1363

56. Li, S., Covino, N. D., Stein, E. G., Till, J. H., and Hubbard, S. R. (2003) *J. Biol. Chem.* **278,** 26007–26014

57. Parast, C. V., Mroczkowski, B., Pinko, C., Misialek, S., Khambatta, G., and Appelt, K. (1998) *Biochemistry* **37,** 16788–16801

58. Cheetham, G. M. (2004) *Curr. Opin. Struct. Biol.* **14,** 700–705

59. Tegge, W. J., and Frank, R. (1998) *Methods Mol. Biol.* **87,** 99–106

60. Wang, W., Marimuthu, A., Tsai, J., Kumar, A., Krupka, H. I., Zhang, C., Powell, B., Suzuki, Y., Nguyen, H., Tabrizizad, M., Luu, C., and West, B. L. (2006) *Proc. Natl. Acad. Sci. U. S. A.* **103,** 3563–3568

61. McTigue, M. A., Wickersham, J. A., Pinko, C., Showalter, R. E., Parast, C. V., Tempczyk-Russell, A., Gehring, M. R., Mroczkowski, B., Kan, C. C., Villafranca, J. E., and Appelt, K. (1999) *Structure* **7,** 319–330

62. Blencke, S., Zech, B., Engkvist, O., Greff, Z., Orfi, L., Horvath, Z., Keri, G., Ullrich, A., and Daub, H. (2004) *Chem. Biol.* **11,** 691–701

63. Liu, Y., Shah, K., Yang, F., Witucki, L., and Shokat, K. M. (1998) *Bioorg. Med. Chem.* **6,** 1219–1226

64. Schlessinger, J. (2003) *Science* **300,** 750–752

65. Stamos, J., Sliwkowski, M. X., and Eigenbrot, C. (2002) *J. Biol. Chem.* **277,** 46265–46272

66. Lougheed, J. C., Chen, R. H., Mak, P., and Stout, T. J. (2004) *J. Biol. Chem.* **279,** 44039–44045

67. Ogiso, H., Ishitani, R., Nureki, O., Fukai, S., Yamanaka, M., Kim, J. H., Saito, K., Sakamoto, A., Inoue, M., Shirouzu, M., and Yokoyama, S. (2002) *Cell* **110,** 775–787

68. Bongarzone, I., Vigano, E., Alberti, L., Borrello, M. G., Pasini, B., Greco, A., Mondellini, P., Smith, D. P., Ponder, B. A. J., Romeo, G., and Pierotti, M. A. (1998) *Oncogene* **16,** 2295–2301

69. Borrello, M. G., Smith, D. P., Pasini, B., Bongarzone, I., Greco, A., Lorenzo, M. J., Arighi, E., Miranda, C., Eng, C., Alberti, L., Bocciardi, R., Mondellini, P., Scopsi, L., Romeo, G., Ponder, B. A. J., and Pierotti, M. A. (1995) *Oncogene* **11,** 2419–2427

70. Mol, C. D., Dougan, D., Schneider, T. R., Skene, R. J., Kraus, M. L., Scheibe, D. N., Snell, G. P., Zou, H., Sang, B. C., and Wilson, K. P. (2004) *J. Biol. Chem.* **279,** 31655–31663

71. Zhang, X., Gureasko, J., Shen, K., Cole, P. A., and Kuriyan, J. (2006) *Cell* **125,** 1137–1149

72. Paratcha, G., Ledda, F., Baars, L., Coulpier, M., Besset, V., Anders, J., Scott, R., and Ibáñez, C. F. (2001) *Neuron* **29,** 171–184

73. Bishop, A. C., Ubersax, J. A., Petsch, D. T., Matheos, D. P., Gray, N. S., Blethrow, J., Shimizu, E., Tsien, J. Z., Schultz, P. G., Rose, M. D., Wood, J. L., Morgan, D. O., and Shokat, K. M. (2000) *Nature* **407,** 395–401

74. Manley, P. W., Cowan-Jacob, S. W., and Mestan, J. (2005) *Biochim. Biophys. Acta* **1754,** 3–13

75. Carlomagno, F., and Santoro, M. (2004) *J. Chemother.* **16,** Suppl. 4, 49–51

76. Santoro, M. M., Penengo, L., Minetto, M., Orecchia, S., Cilli, M., and Gaudino, G. (1998) *Oncogene* **17,** 741–749

77. Jeffers, M. F. (1999) *Oncogene* **18,** 5120–5125

78. Uchino, S., Noguchi, S., Adachi, M., Sato, M., Yamashita, H., Watanabe, S., Murakami, T., Toda, M., Murakami, N., and Yamashita, H. (1998) *Jpn. J. Cancer Res.* **89,** 411–418

79. Wallace, A. C., Laskowski, R. A., and Thornton, J. M. (1995) *Protein Eng.* **8,** 127–134